RSC Advances

Facile hydrothermal synthesis of flower-like Co-doped NiO hierarchical nanosheets as anode materials for lithium-ion batteries

Journal:	*RSC Advances*
Manuscript ID	RA-ART-08-2015-017017.R1
Article Type:	Paper
Date Submitted by the Author:	29-Sep-2015

Complete List of Authors:	Xu, Hui; Southwest University of Science and Technology, Zeng, Min; Southwest University of Science and Technology, State Key Laboratory Cultivation Base for Nonmetal Composites and Functional Materials Li, Jing; Southwest University of Science and Technology, State Key Laboratory Cultivation Base for Nonmetal Composites and Functional Materials Tong, Xiaoling; Southwest University of Science and Technology,

Subject area & keyword:	

Journal Name

ARTICLE

Facile hydrothermal synthesis of flower-like Co-doped NiO hierarchical nanosheets as anode materials for lithium-ion batteries

Received 00th January 20xx,
Accepted 00th January 20xx

DOI: 10.1039/x0xx00000x

www.rsc.org/

Hui Xu, Min Zeng*, Jing Li and Xiaoling Tong

Co-doped NiO hierarchical nanosheets with a flower-like morphology were synthesized using a facile hydrothermal process and characterized systematically by X-ray diffraction, X-ray photoelectron spectroscopy, field-emission scanning electron microscopy, energy dispersive X-ray spectrometer and electrochemical measurements. The assembled Co-doped NiO electrode was found to deliver an initial discharge capacity of 1487.5 mAh g^{-1} and it retained a reversible capacity of up to 708 mAh g^{-1} after 50 cycles at a current density of 0.1 C (1 C = 718 mAh g^{-1}). By contrast, a pristine NiO electrode tested under the same conditions delivered a reversible capacity of 128.7 mAh g^{-1} after 50 cycles. The doped electrode also exhibited a high Coulomb efficiency, excellent cycle stability and good rate capability when compared with an undoped electrode. This improved electrochemical performance is attributed primarily to the efficient substitution of Co^{2+} for Ni^{2+} in the metal oxide matrix, which enhanced the p-type conductivity of NiO by the generation of free holes in the valence band. Moreover, the novel nanosheet structure was also able to enlarge the electrode/electrolyte contact area and shorten the path length for lithium ion transport. It is reasonable to conclude that the reported superior lithium storage capacity Co-doped NiO hierarchical nanosheets can be promising new anode material for high-performance lithium-ion batteries.

Introduction

Future development of electric vehicles will require improvements to large-scale energy storage devices. Lithium-ion batteries (LIBs) are considered to be the most promising candidate for this purpose due to their substantial advantages including, high energy density, long cycle life, low self-discharge, no memory effect and environmental friendliness.[1,2] However, the conventional graphite anode in LIBs suffers from low theoretical capacity (372 mAh g^{-1}), low tap density (2.27 g cm^{-3}) and poor rate capability, which will become obstacles for future use of graphite as a power battery anode material. To circumvent these impediments and meet the increasing requirements for vehicle electrification, it is essential to develop new high-performance anode materials for LIBs.[3] Recently, transition metal oxides (NiO,[4] MnO_2,[5] Fe_2O_3,[6] Co_3O_4[7]) have shown great promise the anode materials for LIBs due to their latent advantages. Among transition metal oxides, NiO is one of the more favored candidates due to its high theoretical capacity (718 mAh g^{-1}), high tap density (6.81 g cm^{-3}), enhanced safety and widespread availability.[8] Unfortunately, its low electrical conductivity and intrinsically induced drastic volume change result in a loss of charge transfer and electrode pulverization, which lead to a rapid capacity decay, poor cycling stability and rate capability.[8,9]

A variety of strategies have been developed to overcoming these drawbacks, in particular improving the electrical conductivity of NiO by the synthesis of nanoscale NiO[4,9] and development of carbon-based composites.[8,10,11] To this end, a recent report detailed synthesis of NiO anode materials containing holes in the NiO matrix.[12,13] As an intrinsic p-type semiconductor with a relatively large band gap (~3.6 eV), the hole concentration of NiO plays a crucial role in improving its electrical conductivity of this material. Generally speaking, metal doping can effectively increase the electrical conductivity of this NiO by the substitution of other metal ions for Ni^{2+} ions, which generate excess holes in the valence band of NiO.[14] Here we report a facile hydrothermal strategy to synthesize flower-like Co-doped NiO nanosheets as an advanced anode material for high-performance LIBs. It was expected that Co^{2+} ions would diffuse into the NiO lattice and partially substitute for Ni^{2+} ions, resulting in an increase the hole concentration of p-type NiO nanosheets, thereby enhancing the electrical conductivity of the material. In addition, electrochemical investigations of this new material indicated that the doped electrodes possess a low charge-transfer resistance, a high reversible capacity, excellent cycling stability and good rate capability.

Experimental

Synthesis of flower-like Co-doped NiO nanosheets

School of Materials Science and Engineering, Southwest University of Science and Technology, Mianyang 621010, P R China. E-mail: zengmin@swust.edu.cn
† Footnotes relating to the title and/or authors should appear here.
Electronic Supplementary Information (ESI) available: [details of any supplementary information available should be included here]. See DOI: 10.1039/x0xx00000x

Co-doped NiO nanosheets with a flower-like morphology (denoted as Co-NiO) were synthesized using a facile hydrothermal process with subsequent calcination. In brief this process consisted of initially adding 1.42 g of $NiSO_4$•$6H_2O$ and 0.14 g of $CoCl_2$•$6H_2O$ to 50 mL of ultrapure water in a flask together with 14 mL of N, N-dimethylformamide (DMF) and 7 mL of trifluoroacetic acid (TFA). The mixture was then vigorously stirred for 30 min to dissolve the components. Subsequently, the reaction mixture was transferred to a 100 mL Teflon-lined autoclave, then sealed and heated at 180 °C for 24 h. The resulting precipitates were centrifuged and washed thoroughly with ultrapure water and then dried at 60 °C for 12 h under vacuum. The product was calcined at 500 °C for 5 h in air to enhance its crystallinity. For comparison, pristine NiO was also prepared using the same conditions, but without the presence of $CoCl_2$•$6H_2O$.

Materials Characterizations

The samples were initially characterized by X-ray diffraction (XRD) using an X-ray diffraction analyzer with Cu-Kα radiation (X´Pert PRO, PANalytical). X-ray photoelectron spectroscopy (XPS) measurements were performed on the product using a VG MultiLab 2000 system with a monochromatic Al Kα X-ray source (Thermo VG Scientific). The morphology and composition of the products were examined using field emission scanning electron microscope (Ultr55, Zeiss) equipped with energy dispersive X-ray spectrometer (EDX).

Electrochemical Measurements

The electrochemical performance of the novel material was determined using CR2016-type coin cells. The working electrodes were fabricated by mixing the active materials with super P and polyvinylidene difluoride (PVDF) in a weight ratio of 8:1:1 and then milling the mixture homogeneously in an agate mortar. Subsequently, an appropriate amount of N-methylpyrrolidone solvent was slowly introduced to the wet mixture to produce a slurry. The uniform slurry was coated onto a copper foil using a scraper and dried at 120 °C for 24 h. These electrodes were punched into disks and assembled into half cells in an Ar-filled glove box. Li foils were used as the counter electrodes and the polypropylene microporous films were employed as the separators. The commercial electrolyte was used which contained 1 M solution of $LiPF_6$ in dimethyl carbonate and ethylene carbonate with in a volume ratio of 1:1. Cyclic voltammetry measurements were performed using a CHI760C electrochemical station in the voltage range of 0 to 3.0 V (*vs*. Li/Li^+) at a scan rate of 0.1 mV s^{-1}. The galvanostatic charge-discharge measurements were conducted using a LAND battery test system in the voltage range of 0.01 to 3.0 V (*vs*. Li/Li^+) at different current densities. Electrochemical impedance spectroscopy measurements were also carried out using a CHI760C electrochemical station in the frequency range of 0.01 Hz to 100 KHz.

Results and discussion

The XRD patterns of pristine NiO and Co-NiO are shown in Figure 1. The characteristic diffraction peaks of both samples correspond to the (111), (200), (220), (311) and (222) planes of well-crystallized cubic NiO. There were no impurity peaks for cobalt oxides or other impurities detected in the XRD results for the Co-NiO, implying that the Co doping did not change the original NiO structure. However, it should be noted that the diffraction peaks of the Co-NiO showed a slight shift to higher angles as Co was introduced into the NiO lattice, suggesting an efficient substitution of Co^{2+} for Ni^{2+}, which caused a small lattice contraction of the NiO matrix due to the smaller ionic radius of Co^{2+} (0.65 Å) than Ni^{2+} (0.69 Å).[14,15] The corresponding lattice constant was then calculated according to the Bragg's formula. The results showed that the lattice constant was 4.1797 Å for pristine NiO and 4.1767 Å for Co-NiO. Because the cubic lattice structure of NiO is the same as to NaCl, the bond length is equal to the lattice constant, which also indicated that the bond length decreased after Co doping. Furthermore, it is reasonable to assume that the Co^{2+} ions uniformly dispersed into the NiO lattice, which produced more Ni^{2+} vacancies in the lattice and thus contributed to the generation of a vast number of free holes in the valence band, resulting in improved electrical conductivity for the NiO.[16]

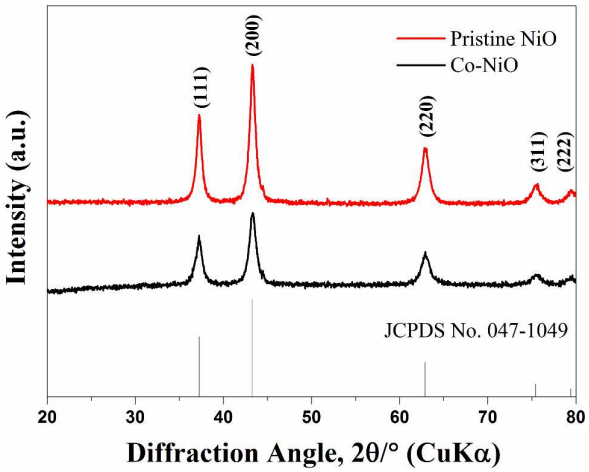

Figure 1. XRD patterns of pristine NiO and Co-NiO.

Additional information about the structure and oxidation states of pristine NiO and Co-NiO was obtained from the X-ray photoelectron spectroscopy (XPS) analysis. Figure 2 (a) shows the XPS wide spectrum of the both samples, which revealed the presence of nickel, cobalt and oxygen in the doped sample. The Co 2p characteristic peaks of CoO can be detected in the inset of Figure 2 (a), indicating the existence of CoO in the Co-NiO.[17] The 3/2 spin–orbit components of the Ni 2p ionization region for pristine NiO and Co-NiO are exhibited in Figure 2 (b) and (c), respectively. The recorded spectra show three peaks at around 854, 855.8 and 860.8 eV (marked as A, B and C), corresponding to the Ni^{2+}, Ni^{3+} and satellite structures,[18,19] which clearly indicated that Ni was present at the surface of the both samples. This was mainly in the Ni^{2+} state with a slight contribution of Ni^{3+} and no metallic Ni was observed.[12] It is believed that the presence of Ni^{3+} may result from the exposure of the sample to air. On the other hand, we can infer that the presence of Ni^{3+} refers primarily to the existence of a structure containing Ni^{2+} ions with holes and, hence does not indicate the existence of a Ni_2O_3 phase.[12,18,19] The peak A at 854.1 eV in Co-NiO is close to that of

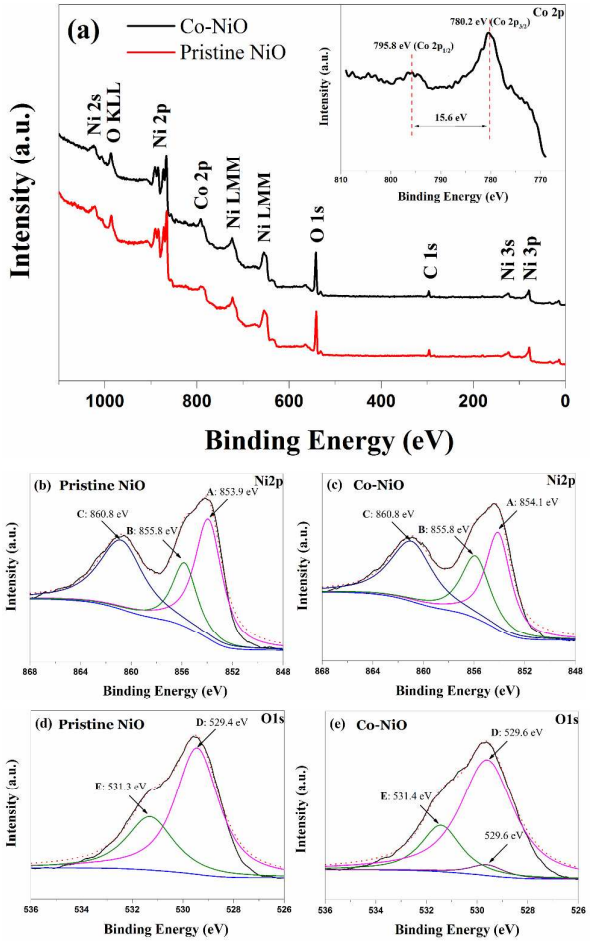

pristine NiO (853.9 eV) with a little shift, suggesting that this larger binding energy in Co-NiO may be due to the substitution of Co^{2+} for

Figure 2. (a) XPS wide spectrum of pristine NiO and Co-NiO, the inset is the Co 2p spectra; (b, c) Ni $2p_{3/2}$ spectra and (d, e) O 1s spectra of pristine NiO and Co-NiO.

Ni^{2+}. This implies that Co doping influences the site environment of the Ni enhancing the electron cloud density of Ni.[20] The intensity ratio of peak A/peak B decreased after Co doping, which also suggests that Co^{2+} was partially substituted for Ni^{2+}, resulting in an increase in hole concentration in Co-NiO.[21] Figure 2 (d) and (e) shows a comparison of the O 1s spectra for pristine NiO and Co-NiO. The peaks at around 529.4 and 531.3 eV (marked as D and E) correspond to the oxygen ions in fully oxidized surroundings and the oxygen ions in oxygen deficient regions, respectively.[12,18,22] It can be seen that the positions of the peaks in Co-NiO also show a slight shift due to the larger binding energy of Ni−O bands after Co doping.[21] Moreover, it was found that the Co-NiO gives rise to one more O 1s peak at 529.6 eV, corresponding to CoO.[13,21] The results of the O 1s spectra agree well with the analysis of the Ni $2p_{3/2}$ spectra.

The morphology and structure of pristine NiO and Co-NiO are illustrated by the field emission scanning electron microscopy (FESEM) analysis. The pristine NiO and Co-NiO exhibited similar appearances with a flower-like morphology and layer-by-layer

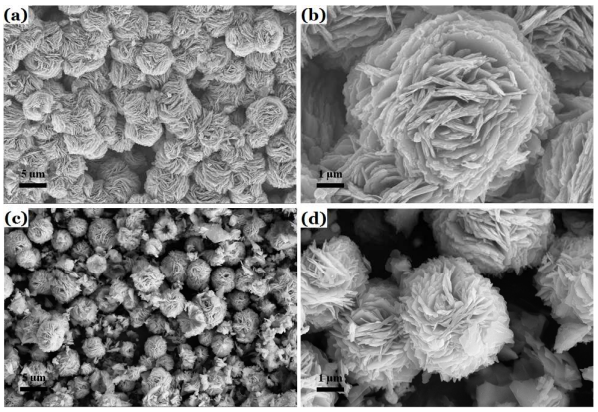

stacked nanosheet structures as observed in the magnified SEM image shown in Figure 3. It can be seen from Figure 3 (a) that the

Figure 3. FESEM images of (a, b) pristine NiO and (c, d) Co-NiO.

pristine NiO exhibited significant agglomeration, resulting in a compact, large secondary flower-like composition as shown in Figure 3 (b). These agglomerated nanosheets had an average size of 4-5 μm with a thickness of about 100 nm, which could lead to poor electrical conductivity due to the long diffusion path for lithium ion transport during cycling. Conversely, the Co-NiO has smaller size (2-3 μm) and thinner nanosheet thickness (~50 nm), although, as shown in Figure 3 (c) and (d), a small number of fragments appeared probably due to collisions during the period of hydrothermal or structural collapse following calcination.[23]. This clearly indicated that the Co doping was helpful in reducing the agglomeration and the thickness of these nanosheets in the Co-NiO sample. Moreover, the relatively smaller and thinner nanosheets with less agglomeration may provide for better rate capability, because of the large surface area, which is beneficial for enlarging the electrode/electrolyte contact area and shortening the path length for lithium ion transport.[13] To further verify the composition and elemental distributions of the doped sample, energy dispersive X-ray (EDX) spectroscopic mapping of Co-NiO was conducted, as shown in Figure 4. The results confirm the presence of Ni, Co and O in the

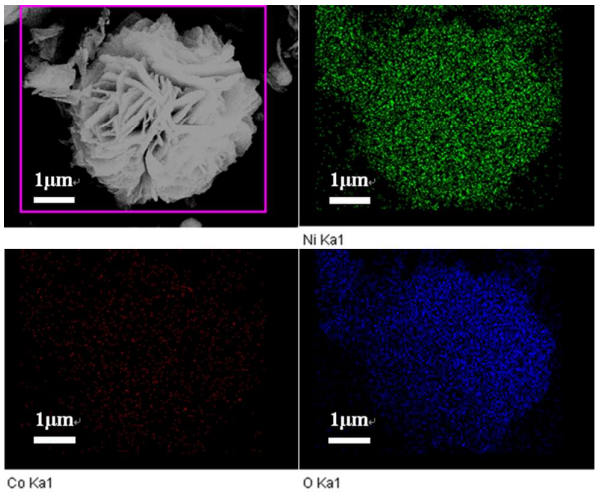

doped sample, which is consistent with the XPS results (Figure 2).

Figure 4. SEM image and the corresponding elemental mapping of Ni, Co and O in the Co-NiO.

The electrochemical performance of the pristine NiO and Co-NiO was initially investigated by cyclic voltammetry at a scan rate of 0.1 mV s^{-1} in the potential range of 0~3 V, as shown in Figure 5. In the first cycle, an obvious cathodic peak at about 0.4 V can be seen for the both samples, which can be attributed to the reduction NiO to Ni, formation of amorphous Li_2O and formation of a partially reversible solid electrolyte interphase (SEI) film whose composition included Li_2CO_3, ethyleneoxide-based oligomers, LiF and lithium alkyl carbonate.[8,13,24] Two anodic peaks at around 1.5 V and 2.2V correspond to the decomposition of the unstable SEI film and Li_2O accompanying with the oxidation of metallic Ni.[8,13,24] The electrochemical reaction mechanism of Li with NiO in Li-ion batteries can be described as:

$$NiO + 2Li^+ + 2e^- \leftrightarrow Ni + Li_2O$$

In addition, it was found that in the first cycle, the current of the cathodic peak for Co-NiO electrode was higher than that for pristine NiO electrode, which is attributed to the improved electrical conductivity of the doped electrode, which promoted the charge transfer needed for the redox process of the formation of an SEI film.[13] The integral area of anodic peak located at about 1.5 V is larger than that for pristine NiO electrode, indicating more dissolution of the SEI organic coating upon the subsequent charge for Co-NiO electrode.[13] In the subsequent cycles, the cathodic peak became broader and shifted to about 0.9 V for the both electrodes, whereas the anodic peaks remained almost unchanged, which is in agreement with the performance of NiO electrodes reported in the literature.[25,26] However, it is important to note that the peak potentials of Co-NiO electrode remained similar and the peak intensity decreased very slightly in comparison to the undoped electrode after the second cycle, which indicated significant reversibility and reproducibility in the doped electrode.[27] Hence, it is reasonable to assume that the Co^{2+} facilitated the Li^+ insertion/desertion in the doped electrode and enhanced the kinetics and the extent of the electrode reactions.

To demonstrate the potential application of the Co-NiO as a LIBs anode, galvanostatic cycling measurements of test cells containing these anodes were performed in the voltage range of 0.01 to 3.0 V at a current density of 0.1C. Figure 6 (a) and (b) show the discharge/charge curves of pristine NiO and Co-NiO in the 1st, 2th, 5th, and 30th cycles. In the first discharge cycle, an extended voltage plateau can be observed at around 0.65 V for both samples, which is a result of the reduction of NiO to Ni and the formation of a partially reversible SEI film.[13,28] During the charge cycle, two voltage plateaus at 1.0–1.5V and 2.0–2.5 V can be observed, corresponding to the decomposition of the SEI film and the reverse reaction of the formation of NiO from Ni and Li_2O.[13,29] These results agree with the CV results. The initial discharge and charge capacities of Co-NiO electrode were 1487.5 and 1052.3 mAh g^{-1}, the initial Coulombic efficiency was 70.7% and this initial large capacity loss was

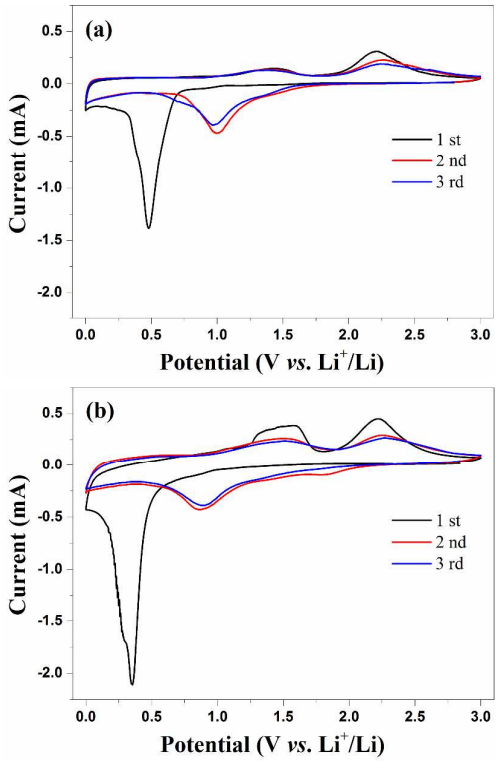

Figure 5. Cyclic voltammograms of (a) pristine NiO electrode and (b) Co-NiO electrode.

due the irreversible lithium loss as a result of surface vacancies and adsorbed trace amounts of water resulting in the formation of an unstable SEI film.[28,30] By contrast, the pristine NiO electrode delivered a reversible capacity of 648.8 mAh g^{-1} for the first cycle and its initial Coulombic efficiency (51.1%) which was also lower than that of the Co-NiO electrode. The improved performance of the doped anode may have been due to the presence of Co^{2+} which made the Li^+ transfer faster and more efficient at the interface, greatly enhancing the reactivity of the electrode reaction.[27] More importantly, the Co-NiO electrode retained a high reversible capacity of 748.8 mAh g^{-1} after 30 cycles, which was far superior to the theoretical capacity of NiO (718 mAh g^{-1}). Based on the electrochemical reaction mechanism, theoretically, 2 Li^+ per NiO were involved in the conversion reaction of NiO. Therefore, the discharge process should consume 2 Li^+ per NiO, but the resulting experimental values for the doped electrode were higher than the theoretical capacity. This extra capacity may be attributed to electrolyte degradation and growth of an electrochemically active polymer-gel-like SEI coating over metal oxide, which increased the material's capacity beyond the theoretical value predicted for the complete reduction of the transition metal oxide to pure metal, as discussed in the literature.[12,27] In addition, a partially reversible SEI film is often the main reason for the low Coulombic efficiency and large capacity loss during the initial cycle, which occurs for nearly all 3d transition metal oxides.[31-33] However, the Coulombic efficiency of Co-NiO soared from 70.7% in the first cycle to 92.9% in the second

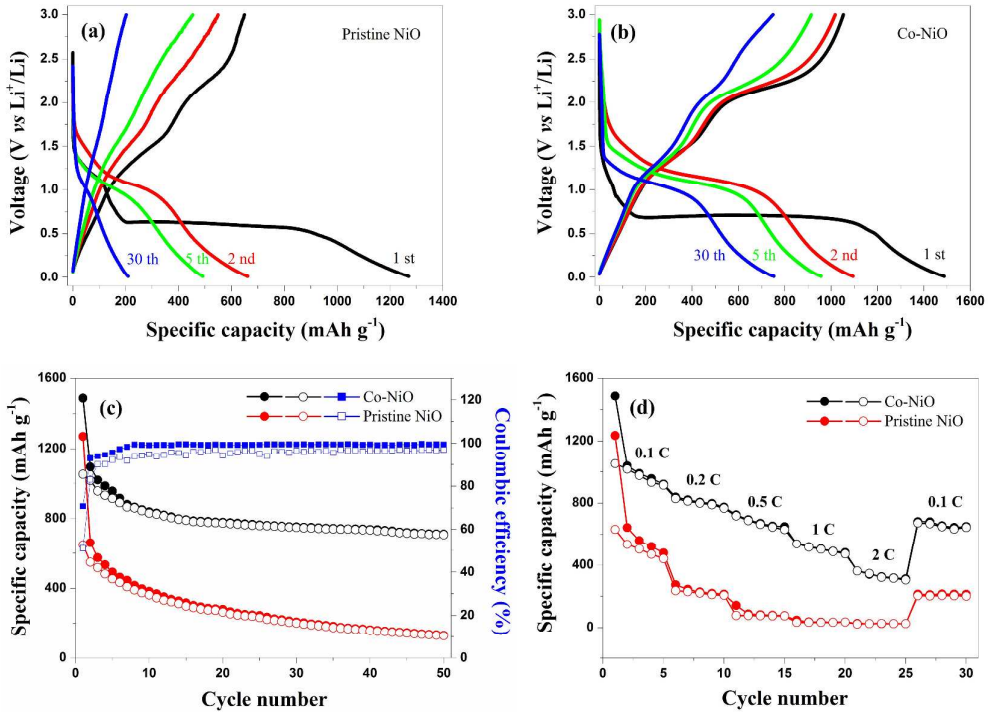

Figure 6. Galvanostatic charge-discharge curves of (a) Pristine NiO and (b) Co-NiO electrodes, (c) Cycling performance at a current density of 0.1 C, (d) rate capability at various rates of 0.1 C to 2 C.

cycle, 95.6% in the fifth cycle, 99.5% in the 30th cycle and then remained above 99.5% in the subsequent cycles. But the pristine NiO electrode suffered rapid reversible capacity fading and lower Coulombic efficiency. These results indicate that the insertion of Co^{2+} into the NiO lattice is helpful in improving the electronic conductivity along with the Li^+ diffusion kinetic properties during the electrochemical reactions.

Another advantage of the Co-NiO electrode is its highly improved cycling performance. The cycling profiles of pristine NiO and Co-NiO are illustrated in Figure 6 (c). The Co-NiO electrode exhibited much better cycling stability, indicating that Co^{2+} can further improved the cycling performance of NiO due to its high electrical conductivity, decrease the ohmic loss and improved electronic conduction pathways in the doped electrode.[27] Moreover, the high specific capacity and excellent cycling performance of the Co-NiO electrode may resulted from the relatively smaller and thinner, slightly agglomerated nanosheet structure, which may shorten the lithium ion transport distance and enhance the kinetics of conversion reactions. Therefore, it is reasonable to conclude that more of the reversible capacity of Co-NiO is retained above 708 mAh g^{-1} after 50 cycles, while the pristine NiO retained a paltry reversible capacity of 128.7 mAh g^{-1}. In addition, the inferior cycling performance of pristine NiO could also result from its inferior electrical conductivity and the severe aggregation of the NiO nanosheets. It should also be noted that the Coulombic efficiency of the Co-NiO was higher than the pristine NiO during cycling. In addition, the capacity retention of Co-NiO attained 67.3% after 50 cycles, which was also higher than that of pristine NiO (19.8%). In light of these results, it is believed that the large volume change that occured in NiO during cycles, may be ameliorated by the Co^{2+} which acted as an elastic buffer reducing the strain associated with the volume change during Li^+ insertion/desertion process. The Co^{+2} may also minimize electrode pulverization, thereby maintaining electronic contact and guaranteeing good cycling performance and high Coulombic efficiency.[12,27] To substantiate the influence of Co doping on the structural stability and the excellent cycling performance, the morphology of the pristine NiO and Co-NiO after 50 cycles at 0.1 C was examined. As shown in Figure 7, no obvious changes in the morphology can be observed for the Co-NiO electrode (Figure 7 (a, b)), in which the active material, conductive agent and binder are homogeneously distributed, demonstrating the structural integrity of the doped sample after cycling. By contrast, serious agglomeration and cracks can be seen in the pristine NiO electrode (Figure 7 (c, d)), indicating structural evolution and aggregation of NiO sheets during cycling, which led to rapid capacity fade.

Figure 6 (d) shows the rate capability of pristine NiO and Co-NiO operated at various rates of 0.1 C to 2 C for five cycles at each current density. Compared with pristine NiO, Co-NiO exhibited a much better rate capability, even at a high rate of 2 C, exhibiting a capacity of 321.2 mAh g^{-1}. A capacity of 648.2 mAh g^{-1} was exhibited after 30 cycles at a cycling rate of 0.1 C, also suggesting good rate capability. However, the capacity of the pristine NiO decreased dramatically at higher rate, to as low

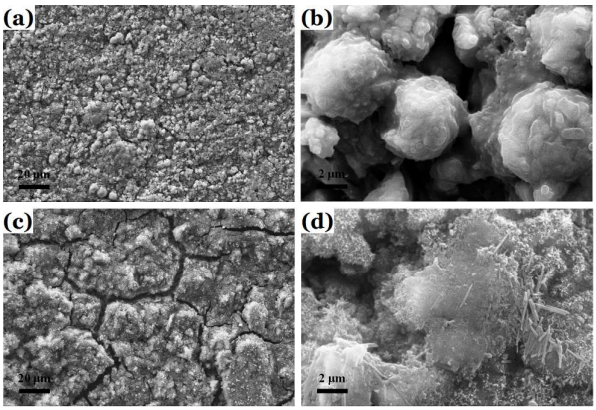

Figure 7. SEM images of (a, b) Co-NiO and (c, d) pristine NiO after 50 discharge/charge cycles.

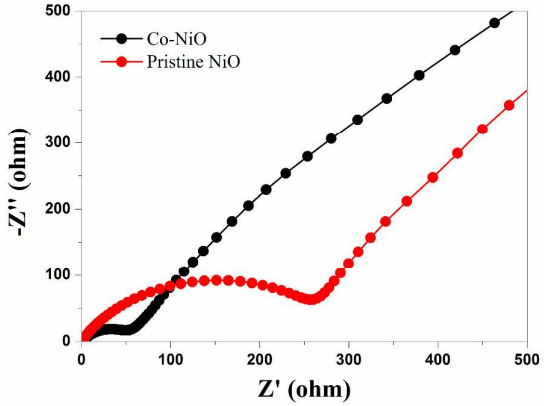

Figure 8. Electrochemical impedance spectra of pristine NiO and Co-NiO.

as 25.6 mAh g^{-1} at 2 C. These results demonstrate that Co^{2+} played a significant role in improving the electrochemical performance of the doped NiO material. The improved cycling performance and rate capability of the doped sample can be attributed to the novel hierarchical nanosheet structure, which contributes to faster diffusion of electrolyte and the high electrical conductivity imparted by the Co^{+2} doping together with the large surface area resulting from diminished agglomeration, favor transport and storage of lithium ions. On the contrary, the severely agglomerated nanosheets and the inferior electrical conductivity of the pristine NiO may account for its poor electrochemical performance. This was probably due of the longer diffusion distance required for the lithium ion resulting in high charge transfer resistance. To improve electrochemical performance of NiO-based anode materials, many concepts have been attempted, such as porous NiO fibers (638 mAh g^{-1}),[24] NiO nanoflake arrays (600 mAh g^{-1}),[13] NiO hollow spheres (490 mAh g^{-1}).[34] Compared with these approaches, the present investigation synchronously considered improvement of the electrical conductivity and accommodation of the volume change of active materials, which resulted in the Co-NiO electrode material exhibiting better comparable capacity and capacity retention, but also higher Coulombic efficiency, better cycling stability and rate capability.

To gain further insight into the electrical conductivity of the Co-NiO, electrochemical impedance spectroscopy measurements were conducted. As shown in Figure 8, the semicircle diameter of Co-NiO electrode is smaller than that of pristine NiO electrode, indicating a smaller charge-transfer resistance, as well as contact and SEI resistance. These can be attributed to the excellent electrical conductivity of doped sample. Hence, the Co-NiO electrode showed better rate capability compared to the pristine NiO electrode. The high reversible capacity, excellent cycling performance and good rate capability make this novel Co-doped NiO nanosheet a promising anode material of LIBs. The superior electrochemical performance of the Co-NiO electrode can be summarized as follows: (i) The electrical conductivity of doped sample was increased by introducing Co^{2+} ions in the NiO matrix, which generates excess holes in the valence band and thus contributes to reducing the internal resistance of the battery.[35] (ii) The flower-like nanosheets with thin size and slight agglomeration alleviate the volume change of NiO, while efficiently providing active sites for Li insertion/desertion during the charge/discharge process. Both of these attributes are beneficial for enlarging the electrode/electrolyte contact area and shortening the path length for lithium ions transport, which result in superior cycling performance and higher capacity.[36] (iii) It is also believed that the Co^{2+} ions act as an elastic buffer in the doped sample which reduces the strain resulted from the volume change during cycling and prevents electrode pulverization guaranteeing good electrical conductivity and rate capability.[12,27] These results strongly suggest that Co doping and the novel nanosheet structure of the doped NiO material are responsible for enhancing the p-type electronic conductivity resulting in improved electrochemical performance.

Conclusions

In summary, we report here on a facile hydrothermal process to synthesize flower-like Co-doped NiO hierarchical nanosheets as a high-performance anode material for LIBs. The reported experimental results indicate that Co doping effectively improved the electrical conductivity of NiO. The Co-NiO electrode exhibited a higher reversible capacity and Coulombic efficiency than a non-doped NiO electrode, with better cycling performance, rate capability and capacity retention. It is suggested that, the enhanced electrochemical performance of the Co-NiO is partially attributable to its thinner nanosheet structure with diminished agglomeration, which helps to enlarge the electrode/electrolyte contact area and shorten the path length for lithium ion transport. It is reasonable to conclude that the Co-doped NiO hierarchical nanosheets may be a promising candidate for use as an anode of LIBs.

Acknowledgements

This work is financially supported by the Project Sponsored by the Scientific Research Foundation for the Returned Overseas Chinese Scholars, State Education Ministry [2011]-1568.

Notes and references

1 M. Armand and J. M. Tarascon, *Nature*, 2008, **451**, 652−657.
Y. Xia, *RSC Adv.*, 2013, **3**, 3352−3358.
3 H. Li, Z. X. Wang, L. Q. Chen and X. J. Huang, *Adv. Mater*, 2009, **21**, 4593−4607.
4 P. P. Lv, H. L. Zhao, Z. P. Zeng, C. H. Gao, X. Liu, T. H. Zhang, *Appl. Surf. Sci.*, 2015, **329**, 301–305.
5 A. P. Yu, H. W. Park, A. Davies, D. C Higgins, Z. W. Chen and X. C. Xiao, *J. Phys. Chem. Lett.*, 2011, **2**, 1855−1860.
6 X. J. Zhu, Y. W. Zhu, S. Murali, D. C Higgins, Z. W. Chen and X. C. Xiao, *ACS Nano*, 2011, **5**, 3333−3338.
7 Y. S. Luo, D. Z. Kong, J. S. Luo, Y. L. Wang, D. Y. Zhang, K. W. Qiu, C. W. Cheng, C. M. Li and T. Yu, *RSC Adv.*, 2014, **4**, 13241–13249.
8 D. Xie, Q. M. Su, W. W. Yuan, Z. M. Dong, J. Zhang and G. H. Du, *J. Phys. Chem. C*, 2013, **117**, 24121−24128.
9 X. N. Shang, X. W. Li, H. W. Yue, S. Xue, Z. J. Liu, X. Y. Hou, D. Y. He, *Mater. Lett.*, 2015, **157**, 7–10.
10 X. H. Huang, P. Zhang , J. B. Wu, Y. Lin, R. Q. Guo, *Mater. Lett.*, 2015, **153**, 102–105.
11 V. Roberta, H. Jusef, *ChemElectroChem*, 2015, **2**, 988−994.
12 T. V. Thi, A. K. Rai, J. Gim, J. Kim, *J. Power Sources*, 2015, **292**, 23−30.
13 Y. J. Mai, J. P. Tu, X. H. Xia, C. D. Gu, X. L. Wang, *J. Power Sources*, 2011, **196**, 6388–6393.
14 K. Matsubara, S. Y. Huang, M. Iwamoto and W. Pan, *Nanoscale*, 2014, **6**, 688−692.
15 C. C. Huang, F. H. Wang, C. C. Wu, H. H. Huang and C. F. Yang, *Nanoscale Res. Lett.*, 2013, **8**, 206−214.
16 L. T. Anh, A. K. Rai, T. V. Thi, J. Gim, S. Kim, E. C. Shin, J. S. Lee, J. Kim, *J. Power Sources*, 2013, **243**, 891−898.
17 Z. S. Wu, W. C. Ren, L. Wen, L. B. Gao, J. P. Zhao, Z. P. Chen, G. M. Zhou, F. Li and H. M. Cheng, *ACS Nano*, 2010, **4**, 3187−3194.
18 L. Cao, D. Wang, R. Wang, *Mater. Lett.*, 2014, **132**, 357−360.
19 M. Yang, H. F. Pu, Q. F. Zhou, Q. Zhang, *Thin Solid Films*, 2012, **520**, 5884−5888.
2 Z. Y. Guo, X. L. Dong, D. D. Zhou, Y. J. Du, Y. G. Wang and Y.
20 C. C. Chen, Y. N. Huang, C. H. An, H. Zhang, Y. J. Wang, L. F. Jiao and H. T. Yuan, *ChemSusChem*, 2015, **8**, 114 –122.
21 J. H. Zhang, G. F. Cai, D. Zhou, H. Tang, X. L. Wang, C. D. Gu and J. P. Tu, *J. Mater. Chem. C*, 2014, **2**, 7013–7021.
22 L. Cao, L. P. Zhu, Z. Z. Ye, *J. Phys. Chem. Solids*, 2013, **74**, 668–672.
23 D. Li, Q. Qin, X. C. Duan, J. Q. Yang, W. Guo and W. J. Zheng, *ACS Appl. Mater. Interfaces*, 2013, **5**, 9095−9100.
24 B. Wang, J. L. Cheng, Y. P. Wu, D. Wang, D. N. He, *Electrochem. Commun.*, 2012, **23**, 5–8.
25 Q. Li, Y. J. Chen, T. Yang, D. N. Lei, G. H. Zhang, L. Mei, L. B. Chen, Q. H. Li, T. H. Wang, *Electrochim. Acta*, 2013, **90**, 80–89.
26 N. S. Spinner, A. Palmieri, N. Beauregard, L. C. Zhang, J. Campanella, W. E. Mustain, *J. Power Sources*, 2015, **276**, 46−53.
27 T. V. Thi, A. K. Rai, J. Gim, J. Kim, *Appl. Surf. Sci.*, 2014, **305**, 617–625.
28 L. L. Hu, B. H. Qu, L. B. Chen, Q. H. Li, *Mater. Lett.*, 2013, **108**, 92−95.
29 G. M. Zhou, D. W. Wang, L. C. Yin, N. Li, F. Li and H. M. Cheng, *ACS Nano*, 2012, **6**, 3214−3223.
30 A. K. Monda, D. W. Su, Y. Wang, S. Q. Chen, Q. Liu, G. X. Wang, *J. Alloys Compd.*, 2014, **582**, 522–527.
31 B. K. Guo, M. F. Chi, X. G. Sun, S. Dai, *J. Power Sources*, 2012, **205**, 495−499.
32 Y. M. Sun, X. L. Hu, W. Luo and Y. H. Huang, *ACS Nano*, 2011, **5**, 7100−7107.
33 W. B Yue, S. H. Jiang, W. J. Huang, Z. Q. Gao, J. Li, Y. Ren, X. H. Zhao and X. J. Yang, *J. Mater. Chem. A*, 2013, **1**, 6928–6933.
34 X. H. Huang, J. P. Tu, C. Q. Zhang, F. Zhou, *Electrochim. Acta*, 2010, **55**, 8981–8985.
35 R. Palombari, J. Electroanal. Chem., 2003, **546**, 23−28.
36 M. M. Yao, Z. H. Hu, Y. F. Liu, P. P. Liu, Z. H. Ai, O. Rudolf, *J. Alloys Compd.*, 2015, **648**, 414−418.